AGU PUBLICATIONS

Geophysical Research Letters

RESEARCH LETTER
10.1002/2015GL064672

Key Points:
- The mean and variance of atmospheric water vapor flux will intensify under projected climate change
- The high-latitude (Arctic) water vapor flux exhibits the largest percentage increases
- The increased water vapor flux is almost exclusively due to increased low-level specific humidity

Supporting Information:
- Figures S1 and S2 and Tables S1–S3
- Figure S1
- Figure S2

Correspondence to:
D. A. Lavers,
dlavers@ucsd.edu

Citation:
Lavers, D. A., F. M. Ralph, D. E. Waliser, A. Gershunov, and M. D. Dettinger (2015), Climate change intensification of horizontal water vapor transport in CMIP5, *Geophys. Res. Lett.*, *42*, 5617–5625, doi:10.1002/2015GL064672.

Received 21 MAY 2015
Accepted 16 JUN 2015
Accepted article online 18 JUN 2015
Published online 8 JUL 2015

Climate change intensification of horizontal water vapor transport in CMIP5

David A. Lavers[1], F. Martin Ralph[1], Duane E. Waliser[1,2], Alexander Gershunov[1,3], and Michael D. Dettinger[1,4]

[1]Center for Western Weather and Water Extremes, Scripps Institution of Oceanography, University of California, San Diego, La Jolla, California, USA, [2]Jet Propulsion Laboratory, California Institute of Technology, Pasadena, California, USA, [3]CASPO, Scripps Institution of Oceanography, University of California, San Diego, La Jolla, California, USA, [4]Scripps Institution of Oceanography, U.S. Geological Survey, La Jolla, California, USA

Abstract Global warming of the Earth's atmosphere is hypothesized to lead to an intensification of the global water cycle. To determine associated hydrological changes, most previous research has used precipitation. This study, however, investigates projected changes to global atmospheric water vapor transport (integrated vapor transport (IVT)), the key link between water source and sink regions. Using 22 global circulation models from the Climate Model Intercomparison Project Phase 5, we evaluate, globally, the mean, standard deviation, and the 95th percentiles of IVT from the historical simulations (1979–2005) and two emissions scenarios (2073–2099). Considering the more extreme emissions, multimodel mean IVT increases by 30–40% in the North Pacific and North Atlantic storm tracks and in the equatorial Pacific Ocean trade winds. An acceleration of the high-latitude IVT is also shown. Analysis of low-altitude moisture and winds suggests that these changes are mainly due to higher atmospheric water vapor content.

1. Introduction

It is hypothesized that global warming will lead to an intensification of the global water cycle [*Held and Soden*, 2006; *Allan and Soden*, 2008; *O'Gorman and Schneider*, 2009]. When investigating the hydrological consequences of such projected changes, three approaches have generally been taken to yield future scenarios of precipitation and hydrological characteristics and water availability. First, the changing nature of extreme precipitation return periods or the extreme values (tails) of the precipitation distribution in the climate projections have been assessed [*Kharin et al.*, 2013; *Sillmann et al.*, 2013; *Toreti et al.*, 2013; *Chen et al.*, 2014; *Polade et al.*, 2014]. These studies concluded that precipitation extremes will become more commonplace in many regions in the future, with the most extreme events increasing in magnitude. Second, raw and downscaled global circulation model (GCM) outputs have been used to drive hydrological or land surface models [*Das et al.*, 2011; *Arnell and Gosling*, 2013; *Prudhomme et al.*, 2014; *Salathé et al.*, 2014; *Schewe et al.*, 2014] to determine projected river flow regime changes, especially in terms of droughts and floods. Third, synoptic-scale features, such as extratropical cyclones [e.g., *Zappa et al.*, 2013] and atmospheric rivers (ARs) [*Dettinger*, 2011; *Lavers et al.*, 2013; *Warner et al.*, 2015], have been evaluated because these phenomena are known to cause extreme precipitation and floods, as well as being essential for water supply. In particular, future ARs are projected to be more frequent and intense, potentially resulting in larger precipitation totals and flooding over midlatitude landmasses.

Other than the few studies on future ARs, most previous research has not directly considered projected changes in the water vapor transport, a key variable connected to heavy precipitation and floods in the midlatitudes [*Ralph et al.*, 2005, 2006, 2013; *Neiman et al.*, 2008, 2011; *Lavers et al.*, 2011, 2012; *Lavers and Villarini*, 2013; *Ramos et al.*, 2015]. This type of assessment can provide a climatological perspective of how the transport component from source-to-sink regions is projected to change. It is therefore the aim of this article to investigate the vertically integrated horizontal water vapor transport (integrated vapor transport (IVT)) using output from the Climate Model Intercomparison Project Phase 5 (CMIP5) [*Taylor et al.*, 2012]. The employed Eulerian methodology identifies regions where the IVTs, and hence the transport through the atmospheric branch of the water cycle, are projected to change.

2. Data and Methods

Twenty-two GCMs from the CMIP5 archive [*Taylor et al.*, 2012] were used in the analysis (Table S1 in the supporting information) based on their data availability; the chosen models have horizontal resolutions ranging from 1.125° × 1.125° to 2.813° × 2.813°. For each model, three simulations (using ensemble member r1i1p1) were considered: Historical runs over 1979–2005 (on days available between 1 January 1979 and 31 December 2005), and two future emissions scenarios, referred to as Representative Concentration Pathways (RCPs; RCP4.5 and RCP8.5 are named to reflect the radiative forcing change at the end of the 21st century, in Wm^{-2}) over 2073–2099 (on days available between 1 January 2073 and 31 December 2099). The specific humidity (in kg/kg) and zonal and meridional winds (in ms^{-1}) were retrieved at a daily resolution on the 1000, 850, 700, and 500 hPa pressure levels. Vertically integrated horizontal zonal and meridional water vapor transports were then calculated in an Eulerian framework and finally combined into the total water vapor transport (hereafter, IVT) [*Neiman et al.*, 2008]. Although IVT is a vector, for the purposes of this paper, the focus is on the IVT magnitude, not its direction.

Daily averaged specific humidity and zonal and meridional winds on 16 pressure levels between 1000 and 500 hPa were obtained from the European Centre for Medium-Range Weather Forecasts ERA-Interim (ERAI) reanalysis [*Dee et al.*, 2011] over the 1979–2005 period. Data were retrieved on a T128 (N255) reduced Gaussian grid and converted to a regular latitude-longitude grid of approximately 0.7° × 0.7°; the daily ERAI IVT was then calculated [*Neiman et al.*, 2008]. A test was undertaken in which the ERAI IVT was calculated (over 1 January 2005 to 31 March 2005) using the 1000, 850, 700, and 500 hPa pressure levels only. The results when compared to the ERAI IVT using 16 pressure levels showed a mean difference of 1.8 $kg\,m^{-1}\,s^{-1}$ over the whole January to March 2005 period, and thus, we do not consider the difference in vertical discretization between the CMIP5 models and ERAI to affect the results significantly.

The mean, standard deviation, and 95th percentiles of the daily IVT fields at each grid point were calculated for ERAI and for each model on their native grids in the historical and future scenarios for the boreal winter (December, January, and February (DJF)) and boreal summer (June, July, and August (JJA)) seasons. Time steps with no IVT were masked before the statistical analysis, and these were chiefly confined to the Himalayan region and Antarctica. For intermodel comparison these statistics were regridded on to a common 2.5° × 2.5° grid using first-order conservative remapping, and multimodel mean fields (of the 22 models' means, standard deviations, and 95th percentiles) were then calculated. A Welch's *t* test was employed at each grid point between the 22 CMIP5 models' mean, standard deviation, and 95th percentile fields in the historical and RCPs to establish whether the null hypothesis of equal means could be rejected (at the 0.01 significance level) between the means of the historical and future scenarios. Area-weighted global-average mean IVT, specific humidity, and wind changes between the historical and future scenarios were also used to summarize the results; the weights were calculated by taking the cosine of the latitude.

3. Results

The mean, standard deviation, and 95th percentiles of daily IVT in the ERAI over 1979–2005 for DJF and JJA are shown in Figures 1a–1c and Figures 2a–2c, respectively. The North Pacific and North Atlantic storm tracks ("IVT storm tracks"), the equatorial Pacific easterly trade winds, and IVT storm tracks due to eastward propagating extratropical cyclones predominantly between 30°S and 60°S (depending on the season) are evident in the mean fields. A poleward migration of the extratropical IVT storm tracks occurs between each hemispheres' winter and summer seasons (cf. Figures 1a and 2a). Along the eastern coast of Asia, the high IVT in JJA may be in part due to tropical cyclone activity; the Indian Monsoon region is also evident in the mean field (Figure 2a). The variability is generally largest in the midlatitude IVT storm tracks, a feature relating to the variance associated with transitory synoptic-scale eddies (or extratropical cyclones); conversely, there is less IVT variability (compared to the midlatitudes) in the easterly trade winds of the tropics, for example, over the equatorial Pacific, indicating more stationary IVT (Figures 1b and 2b). To characterize high-intensity IVT, which in the midlatitudes is associated with extratropical cyclones [*Zhu and Newell*, 1998; *Ralph et al.*, 2004, 2005, 2006] and is often the cause of extreme precipitation and floods, we investigate the 95th percentiles of the IVT distribution. Figures 1c and 2c show that the 95th IVT percentile patterns are broadly similar to those found in the mean fields (Figures 1a and 2a). By comparing the ERAI

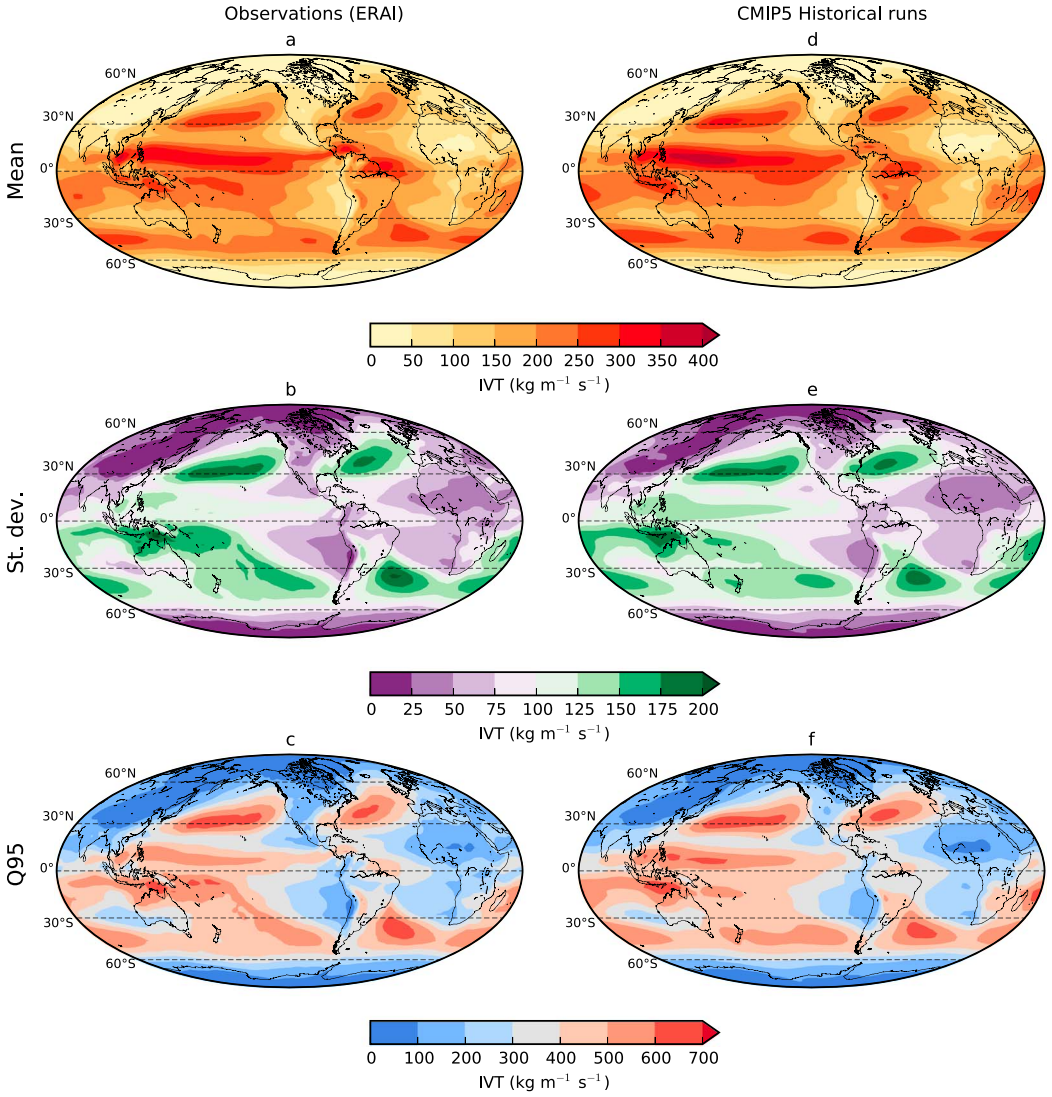

Figure 1. The (a) mean, (b) standard deviation, and (c) 95th percentiles of the DJF days over 1979–2005 in the ERA-Interim reanalysis and from the multimodel mean of (d–f) the 22 CMIP5 historical runs. The statistics are calculated using daily IVT data, and all fields are shown on a common 2.5° × 2.5° grid.

with the multimodel historical mean (calculated from 22 individual model values; Figures 1d–1f and Figures 2d–2f), on average the models capture the intensity and patterns of IVT well, especially in the midlatitudes. This is confirmed by spatial pattern correlations (Spearman rank) of >0.96 between ERAI and the multimodel historical mean for the fields shown in Figures 1 and 2. Note that in JJA the multimodel mean signal has too high IVT over the eastern equatorial Pacific, a troublesome region for climate models [e.g., *Dai*, 2006], but these findings generally give confidence in the mean signal from the 22 models.

The multimodel mean RCP4.5 and RCP8.5 projections of IVT (for DJF over 2073–2099) are shown in Figure 3. Visual inspection of Figures 3a–3f and the multimodel historical mean in Figures 1d–1f show that the mean, standard deviation, and 95th percentiles of IVT increase in the future, a result implying larger vapor transport and an IVT intensification. A Welch's *t* test was employed at each grid point between the 22 model values that comprise the multimodel mean historical and future scenarios to test the null hypothesis of equal means between the historical and future scenarios. In RCP4.5, the regions where the null hypothesis can be rejected at the 0.01 significance level (as given by black dots in Figures 3a–3c) are mainly restricted to IVT regions with large means, standard deviations, and 95th percentiles, but in RCP8.5 with its greater forcing of climatic change, the null hypothesis can be rejected in most places (Figures 3d–3f) providing statistical

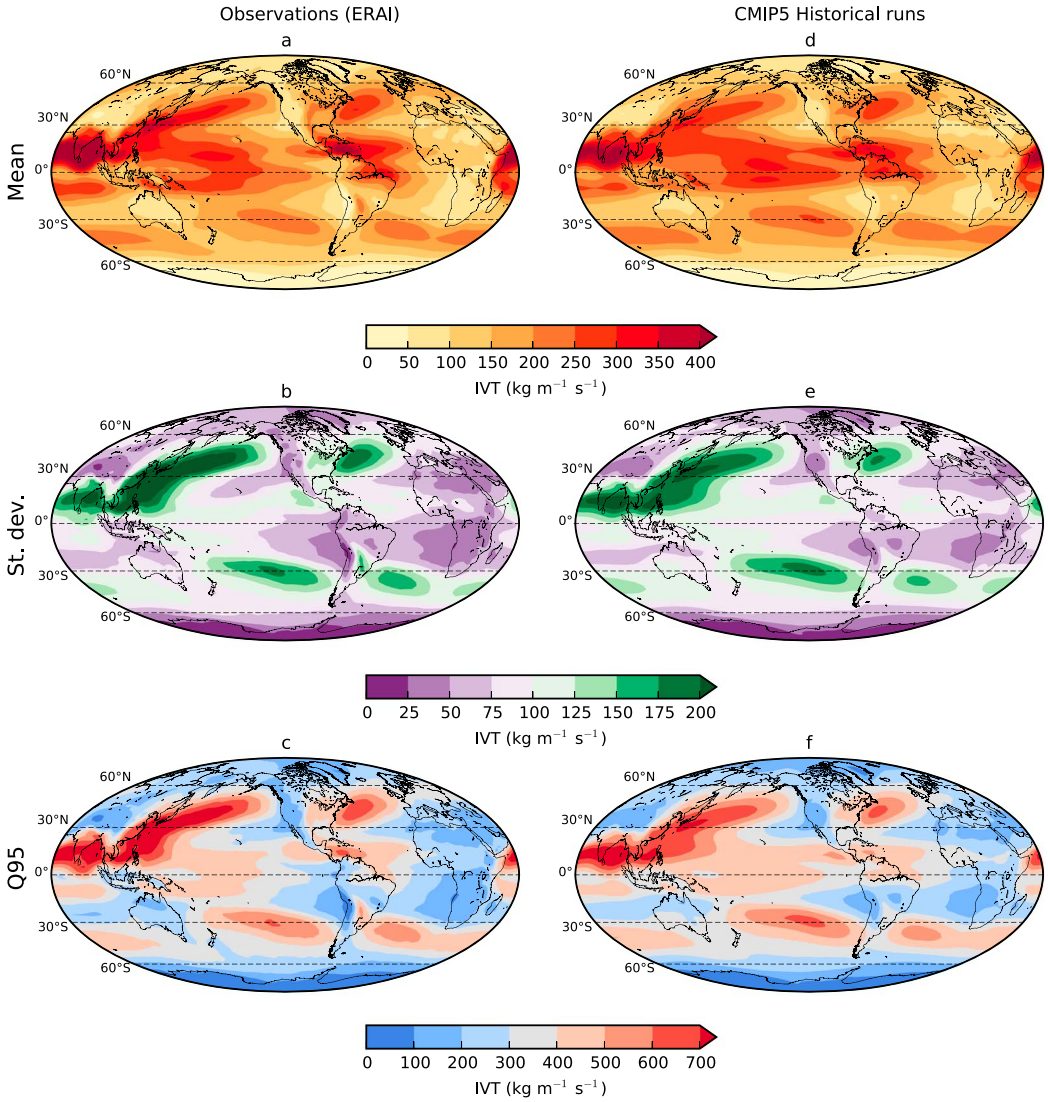

Figure 2. The (a) mean, (b) standard deviation, and (c) 95th percentiles of the JJA days over 1979–2005 in the ERA-Interim reanalysis and from the multimodel mean of (d–f) the 22 CMIP5 historical runs. The statistics are calculated using daily IVT data, and all fields are shown on a common 2.5° × 2.5° grid.

evidence for a projected intensification of the IVT and hence the global water cycle (Table S2 presents the percentage of grid points in DJF where the Welch's *t* test null hypothesis can be rejected). The average IVT percentage increase across the models from the historical to the RCP8.5 scenarios is shown in Figures 3g–3i. All regions, except for the strong subsidence area in the south Pacific high-pressure system off western South America, have increasing IVT, with the Arctic region exhibiting the largest percentage increases (in places approximately 100%). The increasing IVT is likely to be due to higher projected water vapor transport into the Arctic region [e.g., *Bengtsson et al.*, 2011], combined with significant polar warming which will lead to declining sea ice and snow cover, and thus higher evaporation from the Arctic Ocean [*Bintanja and Selten*, 2013]. In JJA, similar IVT increases are found (Figure S1 in the supporting information), and the percentage of grid points where the null hypothesis of the Welch's *t* test can be rejected is higher than in DJF (cf. Tables S2 and S3). No comparable IVT percentage increase is found over Antarctica (consistent with less warming compared to DJF Arctic warming), and smaller IVT increases occur in the Arctic.

Given the relatively zonal IVT orientation, the zonal averages of the percentage increases (relative to the historical simulations) in IVT mean, standard deviation, and 95th percentiles in the two scenarios of each model were calculated to determine the intermodel spread of the IVT intensification (Figure 4). In DJF and

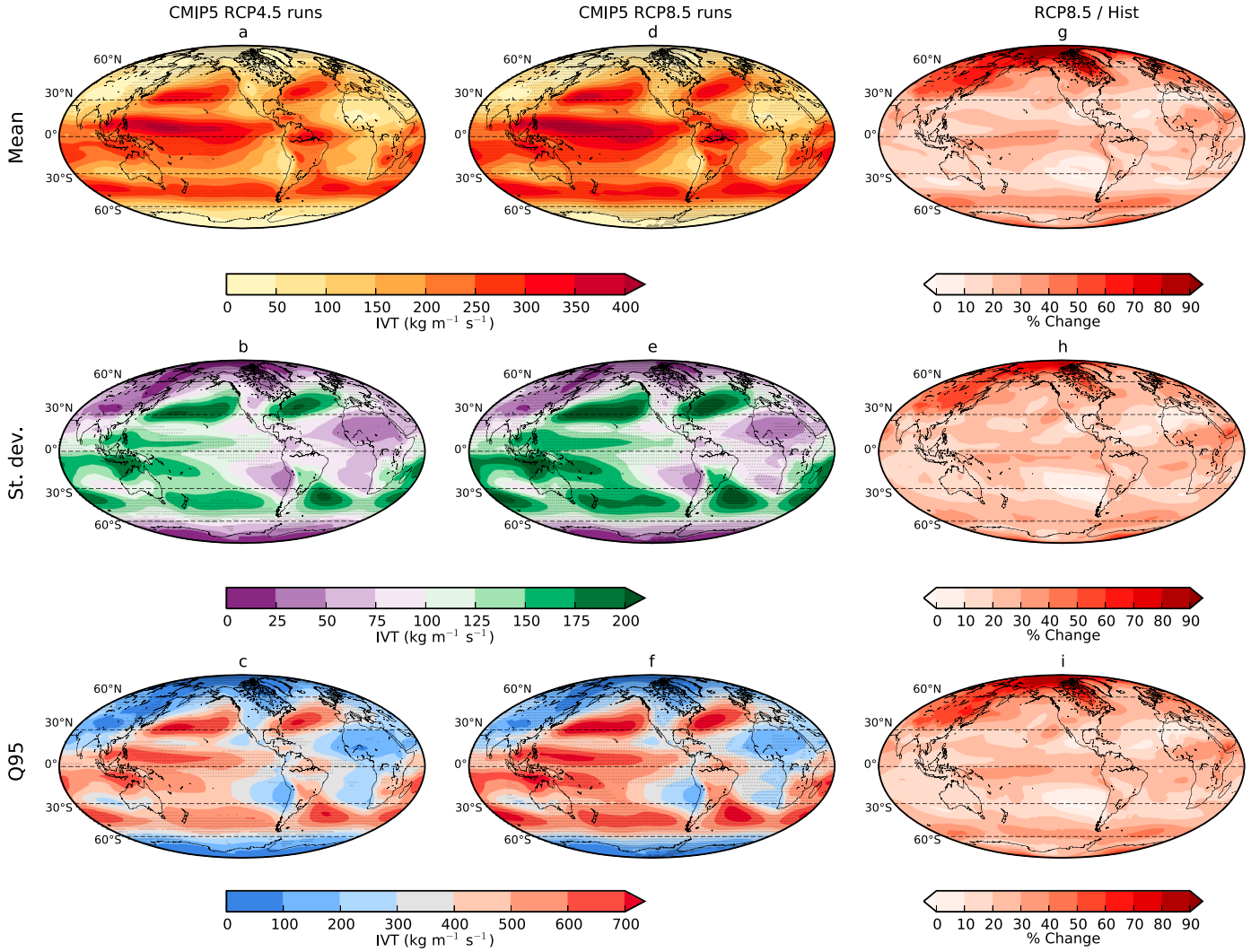

Figure 3. The (a) multimodel mean, (b) standard deviation, and (c) 95th percentiles of the DJF days over 2073–2099 calculated from the 22 CMIP5 RCP4.5 scenarios and calculated from (d–f) the 22 CMIP5 RCP8.5 scenarios. The black dots in Figures 3a–3f represent grid points where the Welch's *t* test null hypothesis for equal means (between the historical runs and future scenarios) is rejected at the 0.01 significance level. (g–i) The mean percentage IVT increases determined from the 22 RCP8.5 scenarios compared to the 22 historical runs are shown. The statistics are calculated using daily IVT data, and all fields are shown on a common 2.5° × 2.5° grid.

JJA, as shown in Figures 4a–4c and 4d–4f, respectively, the IVT statistics increase across most latitudes, with few exceptions (e.g., the subtropical subsidence zones near 30°N). The mean RCP8.5 signal is stronger than that from RCP4.5, although there is overlap between the two scenarios, which is likely to be partly due to the varying climatological biases in the models. Large percentage increases in DJF in the Arctic region again suggest that a warming polar atmosphere will hold more water as vapor, in turn leading to higher IVT. These results show clearly that the transport through the atmospheric branch of the global water cycle is projected to intensify, which for the midlatitudes, corroborates previous studies of future atmospheric rivers [*Dettinger*, 2011; *Lavers et al.*, 2013; *Warner et al.*, 2015]. In midlatitude regions on the west coasts of North America and Europe, the multimodel mean IVT is projected to increase by between 20% and 40% in DJF. With the projected increases in IVT, it is possible that larger precipitation totals will result especially in regions where orographic enhancement of precipitation occurs (e.g., coastal mountains of the western U.S.), and this increasing transport component of the atmospheric water cycle in part explains the projected increase in extreme precipitation found in previous research [*Kharin et al.*, 2013; *Sillmann et al.*, 2013; *Toreti et al.*, 2013; *Chen et al.*, 2014; *Polade et al.*, 2014]. Note that reductions in overall precipitation and precipitation frequency have been projected for the Mediterranean climate regions

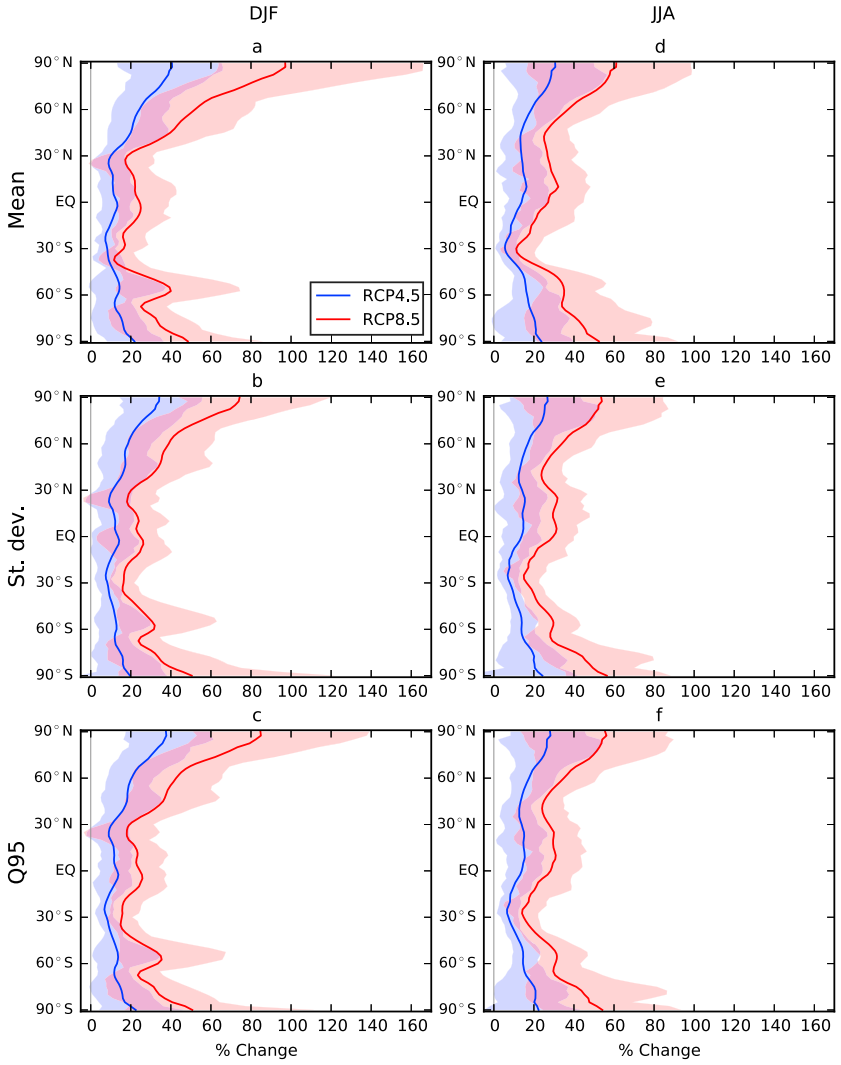

Figure 4. The zonal average percentage changes in the mean, standard deviation, and 95th percentiles IVT for (a–c) DJF and (d–f) JJA from 1979–2005 to 2073–2099. The range of the percentage changes in the RCP4.5 and RCP8.5 scenarios is given by the blue and red envelopes, respectively; the thick blue and red lines are the multimodel mean percentage changes from the RCP4.5 and RCP8.5 scenarios in the 22 CMIP5 models, respectively.

globally [*Polade et al.*, 2014]. It may be that fewer precipitation events will occur in these regions due to a poleward shift in the extratropical cyclone tracks, but when the events do occur, they will have greater IVT. This subject was explored in *Pierce et al.* [2013], which concluded that the large variability in California's projected annual precipitation is due to how the extreme events are handled in different GCMs. Figures 3h-3i suggest that the projected increase in IVT variability and its 95th percentiles should result in higher variability of precipitation and its augmented extremes over California's complex terrain.

We evaluate whether the strengthening IVT is a dynamic (i.e., wind driven) or thermodynamic response to climate change by analyzing the zonal average percentage increases in the statistics of the low-altitude (i.e., 850 hPa, the part of the atmosphere where most vapor transport occurs [*Ralph et al.*, 2005]) specific humidity and wind speed in the two scenarios of each model (compared to the historical runs); the results are shown for DJF in Figure 5. The specific humidity exhibits the clearest increasing signal, with the winds fluctuating about the zero-change line. In RCP8.5, there is a tendency for increasing low-altitude winds at roughly 60°S, a feature that may be related to extratropical cyclone activity over the Southern Ocean. In JJA (Figure S2), a similar signal for increasing 850 hPa specific humidity is found, and, as in DJF, there appears to be a sign of increasing winds over the Southern Ocean. The widespread projected increase in

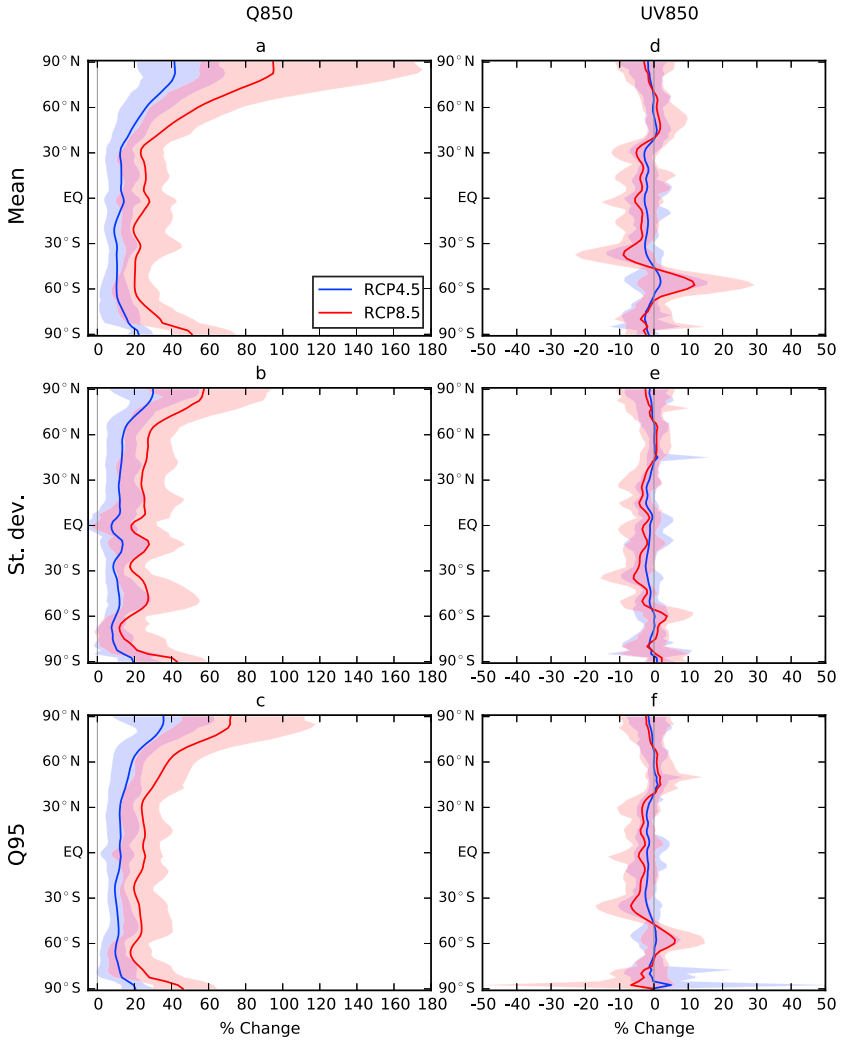

Figure 5. The zonal average percentage changes in the mean, standard deviation, and 95th percentiles for (a–c) 850 hPa specific humidity and (d–f) wind magnitudes in DJF from 1979–2005 to 2073–2099. The range of the percentage changes in the RCP4.5 and RCP8.5 scenarios are given by the blue and red envelopes, respectively; the thick blue and red lines are the multimodel mean percentage changes from the RCP4.5 and RCP8.5 scenarios in the 22 CMIP5 models, respectively. (Values less than 0.001 were masked, so as to guard against extremely high percentage change values.)

low-altitude water vapor content, and the absence of any significant changes to the winds, suggests that the majority of the projected IVT change is a thermodynamic response to a changing climate. We note, however, that there may be some locations where changes in the winds are also important.

4. Summary and Conclusions

We summarize the results by calculating area-weighted global-average multimodel mean IVT changes between the historical and future scenarios. In RCP4.5 and RCP8.5, respectively, the multimodel mean IVT in DJF rises by 11.2 $kg\,m^{-1}\,s^{-1}$ (8.5%) and 22.1 $kg\,m^{-1}\,s^{-1}$ (17.4%), and in JJA, the IVT rises by 13.9 $kg\,m^{-1}\,s^{-1}$ (8.6%) and 27.1 $kg\,m^{-1}\,s^{-1}$ (17.2%). For 850 hPa specific humidity, the area-weighted global-average (in RCP4.5 and RCP8.5, respectively) multimodel mean increases by 9.4% and 19.0% in DJF and by 8.9% and 17.8% in JJA. In comparison, the percentage changes for the mean 850 hPa wind speeds are negative, with values for RCP4.5 and RCP8.5, respectively, of −0.9% and −1.5% in DJF and −0.3% and −0.7% in JJA. Thus, in agreement with Figure 4, at the global scale, the multimodel mean IVT response to increased greenhouse gas concentrations is almost entirely due to commensurate increases in the vapor content of the atmosphere.

The aim of this study was to investigate the IVT in CMIP5 GCMs, in order to understand climatologically how the IVT responds to climate change. Using a straightforward statistical approach the results show that (1) the atmospheric water vapor flux, as given by the mean and 95th percentiles of IVT, will intensify under projected climate change; (2) the high-latitude (Arctic) IVT exhibits the largest percentage increases, especially during DJF; and (3) the IVT variability characterized by the standard deviation will increase. We consider the larger projected IVT to be a reason for the increasing likelihood of extreme precipitation reported in research hitherto [*Kharin et al.*, 2013; *Sillmann et al.*, 2013; *Toreti et al.*, 2013; *Chen et al.*, 2014; *Polade et al.*, 2014], changes that are likely to result in larger and more frequent floods. Results suggest that the changing IVT statistics are predominantly due to increasing low-altitude specific humidity, thus representing a thermodynamic response to climate change, in agreement with the Clausius-Clapeyron equation on the increase in saturation water vapor pressure with air temperature [e.g., *Held and Soden*, 2006]. However, an important caveat is that increased specific humidity cannot alone cause more extreme precipitation; a lifting mechanism, such as frontal or upper level dynamics or a topographic barrier, is required to condense out the water vapor. The methodology employed herein also represents a simple diagnostics tool that could be readily applied in other climate model assessments.

Acknowledgments

We thank Mary Tyree for retrieving the CMIP5 data and California Department of Water Resources for their financial support. D.W.'s contribution was carried out on behalf of the Jet Propulsion Laboratory, California Institute of Technology, under a contract with NASA. Comments from Jonathan Rutz helped improve the manuscript.

The Editor thanks two anonymous reviewers for their assistance in evaluating this paper.

References

Allan, R. P., and B. J. Soden (2008), Atmospheric warming and the amplification of precipitation extremes, *Science*, *321*(5895), 1481–1484.

Arnell, N. W., and S. N. Gosling (2013), The impacts of climate change on river flow regimes at the global scale, *J. Hydrol.*, *486*, 351–364.

Bengtsson, L., K. I. Hodges, S. Koumoutsaris, M. Zahn, and N. Keenlyside (2011), The changing atmospheric water cycle in polar regions in a warmer climate, *Tellus, Ser. A*, *63*, 907–920.

Bintanja, R., and F. M. Selten (2013), Future increases in Arctic precipitation linked to local evaporation and sea-ice retreat, *Nature*, *509*, 479–482.

Chen, H., J. Sun, and X. Chen (2014), Projection and uncertainty analysis of global precipitation-related extremes using CMIP5 models, *Int. J. Climatol.*, *34*, 2730–2748, doi:10.1002/joc.3871.

Dai, A. (2006), Precipitation characteristics in eighteen coupled climate models, *J. Clim.*, *19*, 4605–4630, doi:10.1175/JCLI3884.1.

Das, T., M. D. Dettinger, D. R. Cayan, and H. G. Hidalgo (2011), Potential increase in floods in California's Sierra Nevada under future climate projections, *Clim. Change*, *109*, 71–94, doi:10.1007/s10584-011-0298-z.

Dee, D. P., et al. (2011), The ERA-Interim reanalysis: Configuration and performance of the data assimilation system, *Q. J. R. Meteorol. Soc.*, *137*(656), 553–597.

Dettinger, M. (2011), Climate change, atmospheric rivers, and floods in California—A multimodel analysis of storm frequency and magnitude changes, *J. Am. Water Resour. Assoc.*, *47*(3), 514–523.

Held, I. M., and B. J. Soden (2006), Robust responses of the hydrological cycle to global warming, *J. Clim.*, *19*(21), 5686–5699.

Kharin, V. V., F. W. Zwiers, X. Zhang, and M. Wehner (2013), Changes in temperature and precipitation extremes in the CMIP5 ensemble, *Clim. Change*, *119*(2), 345–357, doi:10.1007/s10584-013-0705-8.

Lavers, D. A., and G. Villarini (2013), The nexus between atmospheric rivers and extreme precipitation across Europe, *Geophys. Res. Lett.*, *40*, 3259–3264, doi:10.1002/grl.50636.

Lavers, D. A., R. P. Allan, E. F. Wood, G. Villarini, D. J. Brayshaw, and A. J. Wade (2011), Winter floods in Britain are connected to atmospheric rivers, *Geophys. Res. Lett.*, *38*, L23803, doi:10.1029/2011GL049783.

Lavers, D. A., G. Villarini, R. P. Allan, E. F. Wood, and A. J. Wade (2012), The detection of atmospheric rivers in atmospheric reanalyses and their links to British winter floods and the large-scale climatic circulation, *J. Geophys. Res.*, *117*, D20106, doi:10.1029/2012JD018027.

Lavers, D. A., R. P. Allan, G. Villarini, B. Lloyd-Hughes, D. J. Brayshaw, and A. J. Wade (2013), Future changes in atmospheric rivers and their implications for winter flooding in Britain, *Environ. Res. Lett.*, *8*, 034010, doi:10.1088/1748-9326/8/3/034010.

Neiman, P. J., F. M. Ralph, G. A. Wick, J. Lundquist, and M. D. Dettinger (2008), Meteorological characteristics and overland precipitation impacts of atmospheric rivers affecting the West Coast of North America based on eight years of SSM/I satellite observations, *J. Hydrometeorol.*, *9*, 22–47, doi:10.1175/2007JHM855.1.

Neiman, P. J., L. J. Schick, F. M. Ralph, M. Hughes, and G. A. Wick (2011), Flooding in western Washington: The connection to atmospheric rivers, *J. Hydrometeorol.*, *12*(6), 1337–1358.

O'Gorman, P. A., and T. Schneider (2009), The physical basis for increases in precipitation extremes in simulations of 21st-century climate change, *Proc. Natl. Acad. Sci. U.S.A.*, *106*(35), 14,773–14,777.

Pierce, D. W., et al. (2013), The key role of heavy precipitation events in climate model disagreements of future annual precipitation changes in California, *J. Clim.*, *26*, 5879–5896.

Polade, S. D., D. W. Pierce, D. R. Cayan, A. Gershunov, and M. D. Dettinger (2014), The key role of dry days in changing regional climate and precipitation regimes, *Nat. Sci. Rep.*, *4*, 4364, doi:10.1038/srep04364.

Prudhomme, C., et al. (2014), Hydrological droughts in the 21st century, hotspots and uncertainties from a global multimodel ensemble experiment, *Proc. Natl. Acad. Sci. U.S.A.*, *111*(9), 3262–3267, doi:10.1073/pnas.1222473110.

Ralph, F. M., P. J. Neiman, and G. A. Wick (2004), Satellite and CALJET aircraft observations of atmospheric rivers over the eastern North-Pacific Ocean during the El Niño winter of 1997/98, *Mon. Weather Rev.*, *132*, 1721–1745.

Ralph, F. M., P. J. Neiman, and R. Rotunno (2005), Dropsonde observations in low-level jets over the northeastern Pacific Ocean from CALJET-1998 and PACJET-2001: Mean vertical-profile and atmospheric-river characteristics, *Mon. Weather Rev.*, *133*, 889–910, doi:10.1175/MWR2896.1.

Ralph, F. M., P. J. Neiman, G. A. Wick, S. I. Gutman, M. D. Dettinger, D. R. Cayan, and A. B. White (2006), Flooding on California's Russian River: Role of atmospheric rivers, *Geophys. Res. Lett.*, *33*, L13801, doi:10.1029/2006GL026689.

Ralph, F. M., T. Coleman, P. J. Neiman, R. Zamora, and M. D. Dettinger (2013), Observed impacts of duration and seasonality of atmospheric-river landfalls on soil moisture and runoff in coastal northern California, *J. Hydrometeorol.*, *14*, 443–459.

Ramos, A. M., R. M. Trigo, M. L. R. Liberato, and R. Tomé (2015), Daily precipitation extreme events in the Iberian Peninsula and its association with atmospheric rivers, *J. Hydrometeorol.*, *16*, 579–597, doi:10.1175/JHM-D-14-0103.1.

Salathé, E. P., Jr., A. F. Hamlet, C. F. Mass, S.-Y. Lee, M. Stumbaugh, and R. Steed (2014), Estimates of twenty-first-century flood risk in the Pacific Northwest based on regional climate model simulations, *J. Hydrometeorol.*, *15*, 1881–1899, doi:10.1175/JHM-D-13-0137.1.

Schewe, J., et al. (2014), Multimodel assessment of water scarcity under climate change, *Proc. Natl. Acad. Sci. U.S.A.*, *111*(9), 3245–3250, doi:10.1073/pnas.1222460110.

Sillmann, J., V. V. Kharin, F. W. Zwiers, X. Zhang, and D. Bronaugh (2013), Climate extremes indices in the CMIP5 multimodel ensemble: Part 2. Future climate projections, *J. Geophys. Res. Atmos.*, *118*, 2473–2493, doi:10.1002/jgrd.50188.

Taylor, K. E., R. J. Stouffer, and G. A. Meehl (2012), An overview of CMIP5 and the experiment design, *Bull. Am. Meteorol. Soc.*, *93*(4), 485–498.

Toreti, A., P. Naveau, M. Zampieri, A. Schindler, E. Scoccimarro, E. Xoplaki, H. A. Dijkstra, S. Gualdi, and J. Luterbacher (2013), Projections of global changes in precipitation extremes from Coupled Model Intercomparison Project Phase 5 models, *Geophys. Res. Lett.*, *40*, 4887–4892, doi:10.1002/grl.50940.

Warner, M. D., C. F. Mass, and E. P. Salathé Jr. (2015), Changes in winter atmospheric rivers along the North American west coast in CMIP5 climate models, *J. Hydrometeorol.*, *16*, 118–128, doi:10.1175/JHM-D-14-0080.1.

Zappa, G., L. C. Shaffrey, K. I. Hodges, P. G. Sansom, and D. B. Stephenson (2013), A multi-model assessment of future projections of North Atlantic and European extratropical cyclones in the CMIP5 climate models, *J. Clim.*, *26*, 5846–5862, doi:10.1175/JCLI-D-12-00573.1.

Zhu, Y., and R. E. Newell (1998), A proposed algorithm for moisture fluxes from atmospheric rivers, *Mon. Weather Rev.*, *126*(3), 725–735, doi:10.1175/1520-0493(1998)126<0725:APAFMF>2.0.CO;2.